remote sensing

MDPI

Article

Evaluation of the Use of UAV-Derived Vegetation Indices and Environmental Variables for Grapevine Water Status Monitoring Based on Machine Learning Algorithms and SHAP Analysis

Hsiang-En Wei [1], Miles Grafton [1,*], Mike Bretherton [1], Matthew Irwin [1] and Eduardo Sandoval [2]

[1] School of Agriculture and Environment, Massey University, Private Bag 11-222, Palmerston North 4442, New Zealand
[2] AgriFood Digital Lab, School of Food and Advanced Technology, Massey University, Private Bag 11-222, Palmerston North 4442, New Zealand
* Correspondence: m.grafton@massey.ac.nz

Abstract: Monitoring and management of grapevine water status (GWS) over the critical period between flowering and veraison plays a significant role in producing grapes of premium quality. Although unmanned aerial vehicles (UAVs) can provide efficient mapping across the entire vineyard, most commercial UAV-based multispectral sensors do not contain a shortwave infrared band, which makes the monitoring of GWS problematic. The goal of this study is to explore whether and which of the ancillary variables (vegetation characteristics, temporal trends, weather conditions, and soil/terrain data) may improve the accuracy of GWS estimation using multispectral UAV and provide insights into the contribution, in terms of direction and intensity, for each variable contributing to GWS variation. UAV-derived vegetation indices, slope, elevation, apparent electrical conductivity (EC_a), weekly or daily weather parameters, and day of the year (DOY) were tested and regressed against stem water potential (Ψstem), measured by a pressure bomb, and used as a proxy for GWS using three machine learning algorithms (elastic net, random forest regression, and support vector regression). Shapley Additive exPlanations (SHAP) analysis was used to assess the relationship between selected variables and Ψstem. The results indicate that the root mean square error (RMSE) of the transformed chlorophyll absorption reflectance index-based model improved from 213 to 146 kPa when DOY and elevation were included as ancillary inputs. RMSE of the excess green index-based model improved from 221 to 138 kPa when DOY, elevation, slope, EC_a, and daily average windspeed were included as ancillary inputs. The support vector regression best described the relationship between Ψstem and selected predictors. This study has provided proof of the concept for developing GWS estimation models that potentially enhance the monitoring capacities of UAVs for GWS, as well as providing individual GWS mapping at the vineyard scale. This may enable growers to improve irrigation management, leading to controlled vegetative growth and optimized berry quality.

Keywords: multispectral UAV; day of the year; elevation; apparent electrical conductivity; slope; weather parameter; elastic net; random forest regression; support vector regression

Citation: Wei, H.-E.; Grafton, M.; Bretherton, M.; Irwin, M.; Sandoval, E. Evaluation of the Use of UAV-Derived Vegetation Indices and Environmental Variables for Grapevine Water Status Monitoring Based on Machine Learning Algorithms and SHAP Analysis. *Remote Sens.* **2022**, *14*, 5918. https://doi.org/10.3390/rs14235918

Academic Editor: Abdul M. Mouazen

Received: 2 November 2022
Accepted: 20 November 2022
Published: 23 November 2022

1. Introduction

Studies have demonstrated that grapevine water status (GWS) is a key factor in berry composition, affecting both vegetative growth and fruit metabolism [1–3]. The berry composition determines the quality at harvest. During the important phenological stages, bloom, and veraison [4], GWS is ideally under controlled water deficit to benefit berry development. This management practice suppresses competition for photosynthetic resources from vegetative growth [5]. In addition, this husbandry promotes the accumulation of sugar and anthocyanins [6] and prevents oxidative damage to canopies resulting from

severe water stress [7]. The fluctuating hydration status in vines varies across vineyards even under a homogeneous irrigation scheme [8], and this subsequently leads to variability in vine growth and berry development [9–11]. To minimize the variation in grape quality across vineyards, it is important to monitor the temporal and spatial variability of GWS while carrying out corresponding practices to keep water status within an optimal range.

Measuring electromagnetic reflectance from plants has become popular because it is associated with physiological status, phenological stage, and other intrinsic variables of the plants [12]. In combination with the use of an unmanned aerial vehicle (UAV), it can provide high spatial resolution images that help further derive vegetation indices (VI) for the whole vineyard in an efficient manner. However, the shortwave infrared band (SWIR, 1–2.5 μm), which has been reported to have an important relationship with foliar water content [13], is not included in most of the commercial and low-cost (lower than USD 5000) UAV-based multispectral sensors [14]. Indices such as water balance index-2 using bands at 0.538 and 1.5 μm are able to identify water stress in grapevines with promising performance (coefficient of determination (R^2) of 0.89) [15]. The inaccessibility of SWIR data has confined the VIs to visible and near-infrared (VNIR) bands, which provide a less satisfying estimation of plant water content [16]. Arevalo-Ramirez et al. [17] found that the SWIR band can be reconstructed from the reflectance of the VNIR band using two machine learning models. Janal et al. [18] tackled the issue from a hardware perspective by developing a multispectral imaging system for UAVs that covers 0.4–1.7 μm of the spectrum. Kandylakis et al. [19] collected spectral data from integrated UAV-based multispectral/SWIR sensors ranging between 0.53–1.7 μm and designed a processing pipeline to execute data analysis for estimating GWS.

Another way to compensate for the missing SWIR band is to utilize the integrated response of plant water status to soil moisture availability, atmospheric demand, plant characteristics, and cultivation practices [20]. A study supports the view that cultivar is the main driver of GWS under well-watered conditions, while vegetative expression and soil type become more dominant as water deficit increases [21]. Weather variables are other important driving factors characterizing the variation of plant water status [22]. These drivers induce hydraulic and metabolic signals that trigger water consumption by crops, along with a range of physiological responses to water deficit, consequently shaping the spatial and temporal variation of GWS in vineyards. Grapevine hydration status is often substituted by predawn leaf water potential (Ψpd), midday stem water potential (Ψstem), midday leaf water potential (Ψleaf), and stomatal conductance. Several studies have been implemented to simulate and explore the relationship between measured GWS and ancillary information composed of vegetative, soil/terrain, temporal, and weather variables [23–28].

To model the relationship between GWS and ancillary information, machine learning techniques offer an attractive alternative due to their ability to model both linear and non-linear systems [29]. These tools are capable of capturing the most informative relationships between inputs and outputs, providing predictions based on a set of data variables having a similar distribution to the training set. To further understand the relationship between inputs and outputs, the prediction capabilities as well as the contribution each input makes to the prediction are of interest. That is, it is important to identify the correlation, as well as the causation, between predictors and response variables. Manipulation may occur when trained models possess logical causation. Preprocessing can be carried out on the input dataset to reduce repetitive information and dependence between predictor variables. In this way, a reasonable causation can be captured while the prediction capacities of the machine learning algorithm may be improved. Interpretability tools, such as Shapley Additive exPlanations (SHAP) [30], are able to provide directionality of the relationships and uncover synergistic effects between multiple variables [31]. When paired with SHAP, machine learning models become more capable as SHAP offers deeper insights into the trained models whose results are usually limited to incomplete interpretation, such as feature importance or variable weight [32].

As vineyard management is strongly linked to the hydration state of vines, an understanding of GWS dynamics and its dominant drivers could be indispensable for viticulture management. The primary goal of this study is to investigate whether the incorporation of ancillary information (weather, temporal, and soil/terrain variables) can enhance the GWS monitoring capacity of UAV-based multispectral sensors without a SWIR band in the production context. The secondary goal is to provide insights into the relationship between GWS and vegetation, weather, temporal, and soil/terrain variables over the flowering-to-veraison period. To the authors' knowledge, this is the first study where GWS monitoring models have been developed in a temperate climate zone in the Southern Hemisphere using ancillary predictors from weather, temporal, and soil/terrain aspects and using SHAP for relationship interpretation. The procedures undertaken were (i) exploring which vegetation indices derived from multispectral imagery are strongly correlated with variation of GWS, with those identified serving as the core input in later modeling, as well as (ii) modeling changes in GWS based on VIs, temporal, soil/terrain, and weather variables. The machine learning model with the best predictive performance and logical causal relationships will then be presented and assessed, (iii) understanding which combination of ancillary variables should be selected in the best performing model, with their contribution and relationship with GWS evaluated using SHAP analysis.

2. Materials and Methods

2.1. The Context of the Study Vineyards and Study Periods

The study's vineyards are located at Martinborough in the Greater Wellington Region in New Zealand (NZ) (Figure 1). The study sites comprise two commercial vineyards owned by Palliser Estate and are named Wharekauhau and Pencarrow. Our study areas within these two vineyards are 6.6 and 6.7 ha, respectively. A S-map online (https://smap.landcareresearch.co.nz/, accessed on 1 April 2022), developed by Landcare Research, was used to provide a basic soil summary (mapped at about 1:50,000) to support the study. There are mainly two types (Glas_8a.2: 60% and Barr_22a.1: 40%) and three types (Barr_22a.1: 50%, Glas_8a.2: 40%, and Waka_26a.1: 10%) of soils across Wharekauhau and Pencarrow, respectively. Glas_8a.2 and Barr_22a.1 have dominant silt texture in their topsoil and subsoil, with gravelly layers from less than 0.45 m to more than 1 m. They are both described as well-drained, with Glas_8a.2 having moderate soil water holding capacity and Barr_22a having high capacity. Waka_26a.1 has silt and clay texture in its topsoil and subsoil, with a gravel content of less than 3% and plant rooting depth extending beyond 1 m. It is described as imperfectly drained and highly vulnerable to water logging, having moderate soil water holding capacity.

Pinot noir was chosen as the target cultivar in this study due to its requirement for relatively precise irrigation management. The Pinot Noir vines in both vineyards were planted in 1998–2000 and trained with two-cane vertical shoot positioning. Inter- and intra-row planting space is 2.2 × 1.7 m for Wharekauhau and 2.2 × 1.8 m for Pencarrow. The annual growth cycle of grapevine in NZ comprises budburst, shoot growth, flowering (September–November), fruit set, and veraison (December–February), followed by berry development and harvesting (March–May). Cultivation practices, such as shoot thinning, bud rubbing, and leaf plucking, are regularly conducted from October to December during the growing season. Between flowering and veraison (termed as the critical period in the following sections), the management of GWS is the most critical determinant in final berry quality.

The trials undertaken in this study took place over two growing seasons. The measurement dates avoided rainy days and matched the most critical period for GWS management. The study periods are between 27 November 2020 and 1 February 2021 for the first growing season and between 29 November 2021 and 21 January 2022 for the second growing season (Figure 2).

Figure 1. Location of study vineyards.

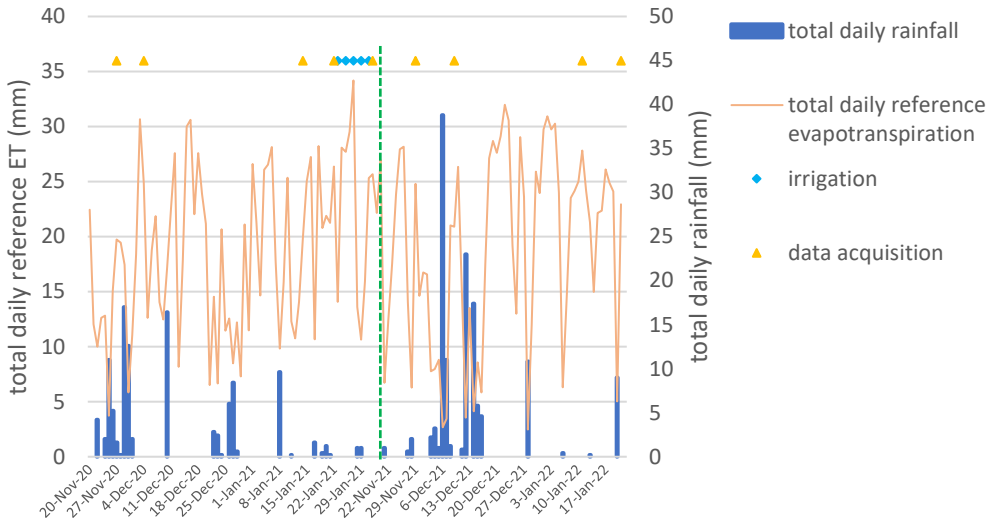

Figure 2. Total daily rainfall recorded by an on-site weather station. Reference evapotranspiration was computed by HARVEST.com (http://harvest.com/, accessed on 1 April 2022) based on the recordings obtained from the weather station. The dates for UAV images and GWS data acquisition were 27 November 2020, 4 December 2020, 14 January 2021, 22 January 2021, 1 February 2021, 29 November 2021, 9 December 2021, 11 January 2022, and 21 January 2022. Irrigation was applied on 23, 25, 27, and 29 January 2021 in the first growing season. The green dash line separates the first and the second growing season.

2.2. Response Variable-Stem Water Potential

Stem water potential (Ψstem) was chosen as a proxy for GWS and has been expressed as a comprehensive indicator for early water deficit in vines during the day [33]. On each measurement date, several healthy vines were sampled in grids to assess variability

across each vineyard (Figure 3) using two mature and fully expanded leaves from the middle part of each sampled canopy. The mature and fully expanded leaves are more representative of the status of canopies. A pressure chamber (model: 610, MPS, Albany, NY, USA) was employed between the hours of 13:00 and 15:30 to assess Ψstem (kPa). Prior to measurement, the sampled leaves were covered with sealable plastic bags for around 1 h. The higher the Ψstem reading, the more dehydrated the vine. These two measurements (per sampled vine) were averaged to represent the vine's canopy water status. A total of 85 and 63 separate canopies were surveyed in the first and the second growing season, respectively, and each of their trunk locations was recorded using a global navigation satellite system (GNSS) with real-time kinematic (RTK) correction (model: GPS1200+, Leica Geosystems AG., Heerbrugg, Switzerland).

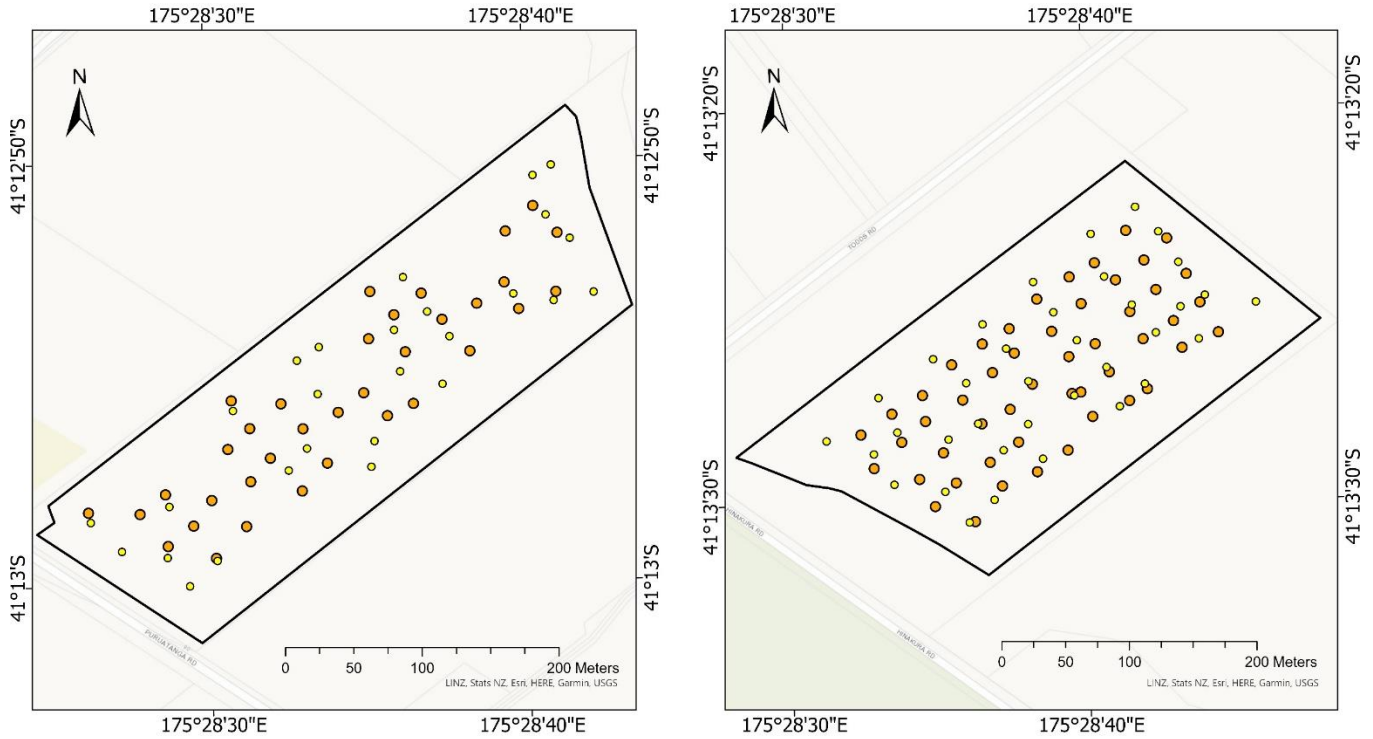

Figure 3. The sampling locations over two study periods. **Left** is the Wharekauhau, and **right** is the Pencarrow vineyards. Orange points represent the observations acquired in the 2020–2021 season, and yellow points represent the observations acquired in the 2021–2022 season.

2.3. Predictor Variable-Vegetation Parameters

Aerial images were obtained between 11:00 and 13:00 under sunny conditions to minimize the influence of sun angle and shadow and to ensure comparability on the same date that Ψstem data were measured. The reflectance, with a spatial resolution of 0.043 m, was recorded by DJI Phantom 4 multispectral UAV (DJI, Shenzhen, China) with six built-in sensors in the blue (450 ± 16 nm), green (560 ± 16 nm), red (650 ± 16 nm), red edge (730 ± 16 nm), and near-infrared (840 ± 26 nm) regions. The DJI Phantom 4 has an integrated sunlight sensor which records irradiance during the flight in the same bands captured by the multispectral sensor for reflectance computing. With this information, UAV images can be normalized, thus allowing for comparison between images taken under different illumination conditions. Photogrammetric processing was applied to the aerial data using Pix4Dmapper (Pix4D SA, Lausanne, Switzerland) to generate digital surface models (DSM), digital terrain models (DTM), and reflectance maps. Settings were designed as follows: key point image was set as full, point cloud densification was set as 1/2 (optimal), and three for image scale, point density, and minimum number of matches, respectively. Classify point cloud was ticked. Noise filtering and surface smoothing using sharp type

were applied. DSMs were produced using an inverse distance weighting algorithm. To increase image spatial accuracy, several ground control points were recorded by GNSS-RTK in each vineyard, and image alignment was subsequently performed in ArcGIS Pro 2.9 (ESRI, Redlands, CA, USA).

The vineyards feature discontinuous vegetation surfaces, so it was necessary to separate canopy pixels from grass and soil pixels to obtain pure information about grapevines. As there is a height difference between grapevine canopies and the surrounding landscape, canopy height was acquired by subtracting DTM from DSM, then creating a binary image with a threshold of 0.9 m to exclude background pixels. For each grapevine, the canopy cordon was set at about 0.8 m from the trunk. Only the vegetation component within 0.5 m distance from the trunk was considered for computing vegetation variables in this study since the shoots of adjacent grapevines are often overlapping and intertwined. The acquisition of specific canopy pixels was carried out by overlapping the buffer zones (using recorded trunk location as the center of a circle with a radius of 0.5 m) with the binary raster of canopy height (Figure 4). Subsequently, 18 vegetation indices for each sampled grapevine, chosen according to frequency of usage in viticulture [34], and shown in Table 1, were calculated based on the mean values of pure canopy pixels using "zonal statistic as table" in ArcGIS Pro.

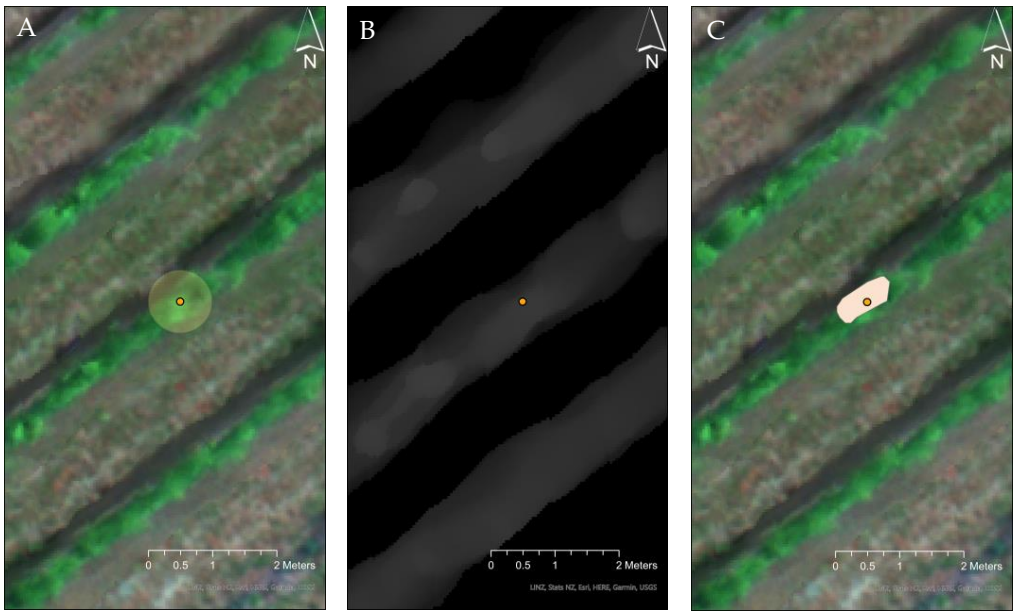

Figure 4. The procedure of getting pure pixels for sampled canopies. (**A**): The subset of an aerial image comprising grapevines and floor vegetation. The buffer zone, the yellow circle, was created according to the recorded location (the orange point) of the sampled grapevine. (**B**): Binary raster of canopy height was generated by subtracting the digital terrain model from the digital surface model. (**C**): Pure grapevine pixels (pink region) were acquired by overlapping the buffer zone with the binary raster.

Table 1. List of vegetation indices used in this study.

Vegetation Index	Acronym	Formula	References
Transformed Chlorophyll Absorption Reflectance Index	TCARI	$3 \times ((\text{Red edge} - \text{Red}) - 0.2 \times (\text{Red edge} - \text{Green}) \times (\text{Red edge}/\text{Red}))$	[35]
Excess Green Index	ExG	$2 \times \text{Green} - \text{Red} - \text{Blue}$	[36]

Table 1. *Cont.*

Vegetation Index	Acronym	Formula	References
Ratio between Transformed Chlorophyll Absorption Reflectance Index and Optimized Soil Adjusted Vegetation Index	TCARI/OSAVI	-	[35]
Normalized Difference Red Edge Index	NDRE	(NIR − Red edge)/(NIR + Red edge)	[37]
Green Normalized Difference Vegetation Index	GNDVI	(NIR − Green)/(NIR + Green)	[38]
Red Edge Chlorophyll Index	CL red edge	(NIR/ Red edge) − 1	[39]
Modified Triangular Vegetation Index	MTVI1	1.2 × (1.2 × (NIR − Green) − 2.5 × (Red − Green))	[40]
Enhanced Vegetation Index	EVI	2.5 × (NIR − Red)/ (NIR + 6 × Red − 7.5 × Blue + 1)	[41]
Difference Vegetation Index	DVI	NIR − Red	[42]
Modified Soil Adjusted Vegetation Index	MSAVI	$(2 \times NIR + 1 - ((2 \times NIR + 1)^2 - 8 \times (NIR - Red))^{1/2})/2$	[43]
Simple Ratio	SR	NIR/Red	[44]
Normalized Difference Vegetation Index	NDVI	(NIR − Red)/(NIR + Red)	[45]
Optimized Soil Adjusted Vegetation Index	OSAVI	(NIR − RED)/(NIR + Red + 0.16)	[46]
Normalized Difference Green/Red Index	NGRDI	(Green − Red)/(Green + Red)	[42]
Red:Green Ratio	R/G index	Red/Green	[47]
Visible Atmospherically Resistant Index	VARI	(Green − Red)/(Green + Red − Blue)	[48]
Modified Chlorophyll Absorption Ratio Index	MCARI	((Red edge − Red) − 0.2 × (Red edge − Green)) × (Red edge/ Red)	[49]
Canopy volume	-	-	[50]

2.4. Predictor Variable-Soil and Terrain Information

An EM38-MK2 is an electromagnetic induction (EMI)-based sensor (Geonics Ltd., Mississauga, ON, Canada). The return reading (apparent electrical conductivity (EC_a)) is considered a function of soil solid types, soil solution, and soil water content [51]. Spatial patterns of EC_a values have been found to be relatively temporally stable between measurement dates [52]. Recommended practice is to undertake measurements when soils are near field capacity and EC_a-based soil variability is at a maximum [53]. In this study, the EM38-MK2 was operated in the vertical dipole mode, with the instrument taking integrated EC_a measurements at about 1.5 m depth. An EMI survey was undertaken on 27 May 2021 by towing the EM38-MK2 at the back of an all-terrain vehicle (less than 0.2 m between EM38-MK2 and the all-terrain vehicle) with a Trimble Yuma tablet incorporating an onboard GPS receiver (model: Yuma, Trimble), accurate to 2–4 m, to geo-reference all point data from the EC_a (mS/m) survey. The vineyards' infrastructure was confirmed with the grower to ensure there was no interference from buried metal components and perched water tables. EC_a points were measured approximately every 3–10 m along transects and 10 m apart, and values less than 0 mS/m were removed before interpolation. The geostatistical interpolation method, empirical bayesian kriging (EBK), was used to transform point data onto a continuous surface raster with 1 m resolution in ArcGIS Pro.

Elevation (m) and slope (degree) information of the location of each sampled canopy was obtained from the 'Wellington LiDAR 1m DEM (2013–2014)' layer provided by the Land Information New Zealand data service (https://data.linz.govt.nz/, accessed on 1 April 2022). This digital elevation model (1 m resolution) was generated by aerial LiDAR captured between 2013 and 2014 for the Greater Wellington region. For each grapevine, the mean values of EC_a, elevation, and slope within 0.5 m distance of the trunk were computed using "zonal statistic as table" in ArcGIS Pro.

2.5. Predictor Variable-Meteorological and Temporal Data

Weather data were recorded by an on-site weather station (175.4741, −41.2247 WGS84) established by HARVEST.com (http://harvest.com/, accessed on 1 April 2022). The target variables include air temperature (°C), relative humidity (%), rainfall (mm), wind speed (km/h), and irradiance (W/m^2). These variables were used to compute mean temperature, mean relative humidity, total rainfall, mean wind speed, and total irradiance based on weekly and daily intervals before each measurement date. It was assumed that climatic conditions were homogeneous across the two vineyards.

2.6. Hierarchical Clustering

One of the goals of this study was to identify causal relationships that may enable growers to utilize or modify GWS according to tailored quality standards. Accordingly, the models developed in this study were required to not only have predictive capabilities, but also logical causality. Initially, all predictor variables were used for regression against Ψstem without clustering preprocessing, so that most of the causal relationships were not intuitive. Subsequent hierarchical clustering was employed to generate groups of highly correlated variables and to produce input datasets with less repetitive information. As a result, the model still exhibits similar prediction results using fewer predictors, and all causal relationships are reasonable and intuitive.

The hierarchical clustering for variables was carried out as an exploratory data analysis [54]. Hierarchical clustering was chosen in this study because it can provide a clear overview of the input datasets in terms of grouping while incorporating expert domain knowledge without the need to pre-specify cluster numbers. This is an important step because repetitive information among variables decreases the precision of machine learning modeling and complicates the interpretation of results. In this study, the similarity between clusters was based on correlation distance, which means that variables which are more positively correlated, based on Pearson correlation, will first merge as one cluster, until all variables are combined into one [55]. The criterion used to determine the distance between two clusters, also called linkage, was set to "complete", referring to the largest dissimilarity between observations in clusters. Hierarchical clustering, regression modeling, and SHAP analysis were implemented with Python 3.9.

2.7. Regression Modeling

On the basis of the clusters generated by hierarchical clustering, combinations of predictor variables were formed by picking one variable from each cluster or not picking any variable from any cluster. All possible combinations, 576 in total, were investigated along with three types of machine learning models for performance comparison. Instead of using conventional variable selection methods such as filtering (e.g., Pearson correlation) or wrapper (e.g., recursive feature elimination), all combinations were evaluated, since the behavior of one variable is influenced by the presence of others. Thus, significant variables would not be removed due to weak correlation with the response variable or having less importance in some of the input datasets. The total samples (n = 148) were split into training (n = 103) and test (n = 45) sets using a 70/30 ratio. This split was carried out and stratified according to the date of measurement to ensure that both training and test sets had corresponding percentages of samples for each date. All predictor variables were standardized to have mean values equivalent to 0 and a standard deviation of 1.

Elastic net (EN), random forest regression (RFR), and support vector regression (SVR) were applied to estimate Ψstem based on climatic, soil/terrain, temporal, and vegetation variables. As the performance of regression models is influenced by their hyperparameters, it was necessary to tune the hyperparameters beforehand to prevent overfitting. This enabled the regression algorithms to exploit their potential. Grid searching on the training set with 10-fold cross-validation was used to search for the best combination of hyperparameters. A list of tuned hyperparameters and their ranges for each algorithm is displayed in Table 2. The test dataset was set aside during hyperparameter tuning and model training. These hyperparameters were then used on the test set for evaluation of the model's generalization performance. To compare the performance of regression models and thus choose the optimal one for further analysis, root mean square error (RMSE) and ratio of performance to interquartile range (RPIQ) values were computed by applying the trained models with the optimized hyperparameters on the test set. Generally, a model with good prediction performance would have larger values of RPIQ and smaller values of RMSE.

Table 2. The tuned hyperparameters and their ranges for each regression model.

Regression Model	Hyperparameter	Range
Elastic net	Constant that multiplies the penalty terms	0.01, 0.1, 1, 10, 100
	Mixing parameter	0.1, 0.2, 0.3, 0.4, 0.5, 0.6, 0.7, 0.8, 0.9
Random forest regression	The number of variables to be considered for the best split	"auto", "sqrt", "log2"
	The maximum depth of the tree	2
	The number of trees in the forest	100
Support vector regression	The used kernel type	"linear", "poly", "rbf"
	Kernel coefficient	"scale", "auto"
	Regularization parameter	0.01, 0.1, 1, 10, 100
	The width of the epsilon-tube	0.1, 0.5, 0.9

Notes: "Auto" refers to the total number of variables, "sqrt" refers to the square root of the total number of variables, "log2" refers to the binary logarithm of the total number of variables, "poly" refers to polynomial, "rbf" refers to radial basis function, "scale" refers to the use of 1/(total number of the variable × variance of the variables) as the kernel coefficient, and "auto" refers to the use of 1/(total number of variable) as the kernel coefficient.

2.8. Shapley Additive Explanations Analysis

The optimal model then underwent SHAP, based on game theory, to explore the relationships and quantify the contribution (SHAP values) of each input according to its average contribution to the model output [30]. In this study, SHAP values based on KernelExplainer were computed for all samples since support vector regression performed the best at modeling and was used in the SHAP analysis. Summary plots for the whole dataset were generated to show important features and the directionality of their impact.

3. Results

3.1. Variation in Stem Water Potential

Both vineyards were visited nine times over two growing seasons, from flowering in late November to veraison in late January. This period is the most critical one before harvest in terms of the effects of GWS on berry quality. Figure 5 displays the variability in Ψstem collected from 148 canopies at two vineyards and the distribution of the measurements on each date. The maximum and minimum observation of Ψstem is 1344 and 293 kPa, respectively. Irrigation was only applied at the end of the study periods in the first growing season (Figure 2). Overall, there is an increasing trend of dehydration in GWS with time in both growing seasons, which indicates the impact of water deficit gradually accumulating

in the canopies. The only exception is an increase in hydration state on 9 December 2021 compared to the previous measurement due to rainfall events a few days before sampling (i.e., 38.8 mm on 6 December 2021 and 11 mm on 7 December 2021). The height of the box and the difference between the upper quartile and lower quartile represent the spatial variation of GWS on one date across each vineyard. Figure 5 demonstrates that it is inappropriate to make irrigation decisions during this period based on single or average measurements collected in the vineyard. This difference became larger as the survey proceeded, which implies spatial variation becomes more obvious when canopies are more dehydrated.

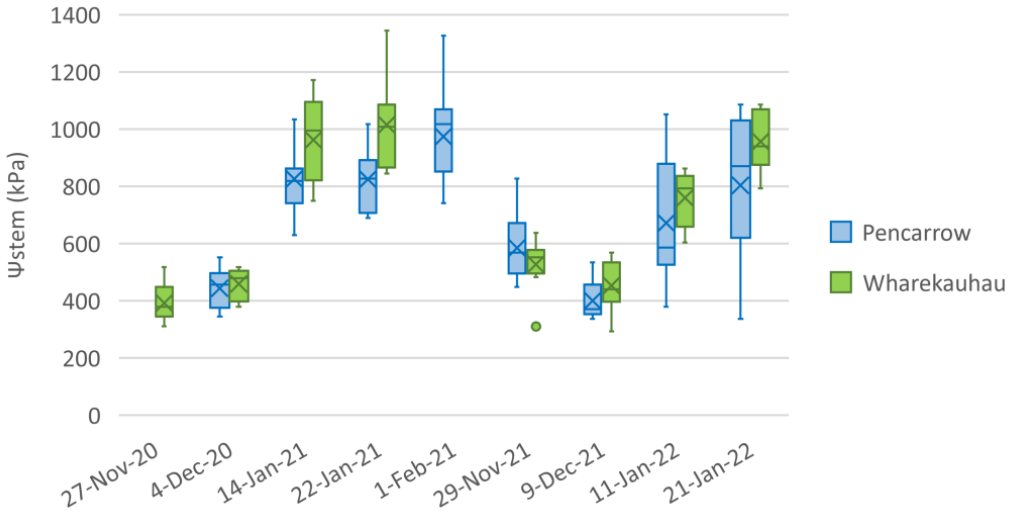

Figure 5. Boxplot of stem water potential (Ψstem) values for the full set of samples collected at Pencarrow (n = 86) and Wharekauhau (n = 62) vineyard. X symbols refer to the average values on the survey dates. Lines in the boxes refer to median values on the survey dates.

3.2. Determination of the Best Descriptor of Vegetation Index for Variation in Grapevine Water Status

According to the goal stated in the introduction section, 18 vegetation indices (VIs) frequently used in viticulture were computed using five bands (i.e., blue, green, red, red edge, and near-infrared) provided by the UAV-based multispectral sensors. VIs were compared with the corresponding Ψstem values recorded in the field surveys to assess their correlation, in terms of R^2 and RMSE, and to check whether changes in Ψstem can be reasonably assessed using drone-based imagery. Amongst all the indices, TCARI had the best linear correlation with variation in GWS, with a R^2 of 0.35 and a RMSE of 213 kPa (Table 3). This was followed by ExG, with a R^2 of 0.3 and a RMSE of 221 kPa. Since TCARI is derived from green, red, and red edge bands, this suggests that TCARI is a promising candidate to help characterize the spatial variation of Ψstem when multispectral sensors are employed. The promising performance of ExG implies that, when only RGB sensors are available, ExG may serve as a spectral indicator for Ψstem. Subsequently, these two indices were used as the core input for separate modeling, with weather, soil/terrain, and temporal variables used to explore the advantage of adding these ancillary variables when regressing against Ψstem.

Table 3. R^2 and RMSE based on a linear regression between GWS and each vegetation index. The vegetation indices are ranked in descending order of R^2. R^2 is coefficient of determination, and RMSE is root mean square error.

Vegetation Index	R^2	RMSE (kPa)
TCARI	0.35	213
ExG	0.30	221

Table 3. *Cont.*

Vegetation Index	R^2	RMSE (kPa)
NDRE	0.25	228
TCARI/OSAVI	0.24	231
GNDVI	0.24	231
CL red edge	0.24	231
Canopy volume	0.19	237
MTVI1	0.16	243
EVI	0.13	247
DVI	0.12	248
MSAVI	0.10	251
SR	0.08	254
NDVI	0.04	258
OSAVI	0.03	260
NGRDI	0.02	262
R/G index	0.02	262
VARI	0.009	263
MCARI	0.0002	264

3.3. Selection of Predictor Variables as Inputs for Modeling Using Hierarchical Clustering

Hierarchical clustering, using correlation distance for distinguishing similarity, was employed to cluster the predictors that were statistically redundant to one another. Later, the model could use any variable from a cluster to form the input dataset. In Figure 6, each leaf of the dendrogram represents one of the 15 predictor variables. The vertical axis indicates how similar the variables are. The earlier (closer to the leaves) that merging between variables occurs, the more positively correlated those variables are. When variables merge close to the top of the dendrogram, the information they contain is nearly independent of each other. The number of clusters was determined by incorporating domain knowledge. As weather variables are intercorrelated and have an impact on plant physiology leading to changes in spectral features (i.e., VIs), it is reasonable to put them into clusters. However, the relationship between soil/terrain variables and short-term weather effects or VIs would be considered weak, so the cut-off line was set at 0.75 for both TCARI and ExG-based models, resulting in eight clusters marked with different colors. The summary for ancillary variables used in this study was listed in Table 4.

Table 4. A summary for all the ancillary variables used to regress against changes in grapevine water status.

Predictor	Abbreviation or Short Name of Predictor	Type
Day of the year	DOY	Temporal
Apparent electrical conductivity	EC_a	Soil/terrain
Elevation	-	Soil/terrain
Slope	-	Soil/terrain
Mean relative humidity	RHmean	Weather
Total rainfall	Rtotal	Weather
Total irradiance	IRtotal	Weather
Mean wind speed	WSmean	Weather
Mean temperature	Tmean	Weather

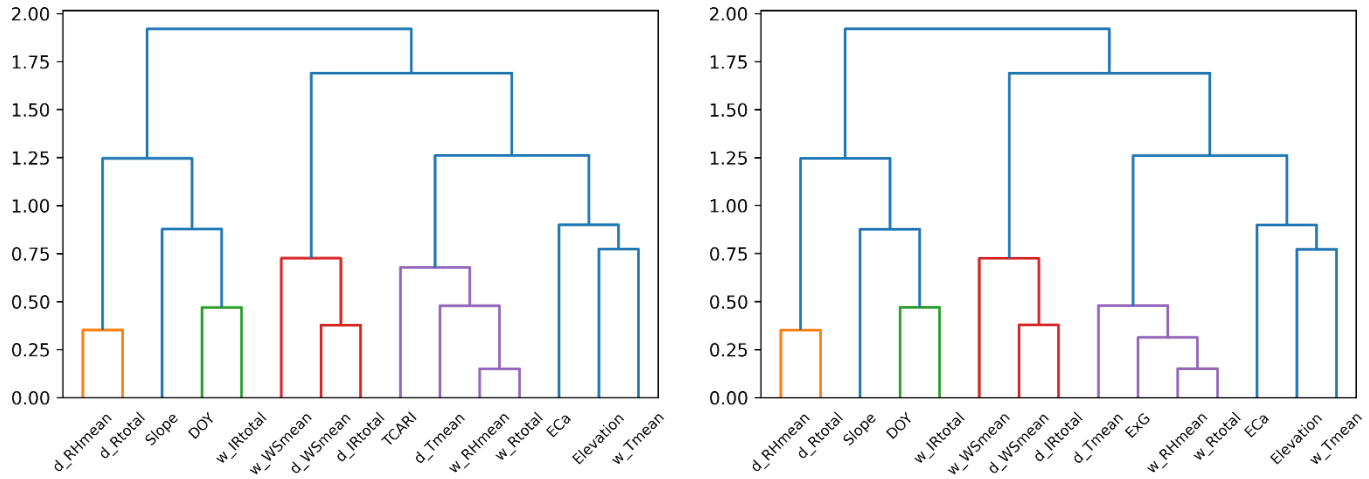

Figure 6. Hierarchical clustering dendrogram of predictor variables: RHmean is mean relative humidity; Rtotal is total rainfall; DOY is day of the year; IRtotal is total irradiance; WSmean is mean wind speed; Tmean is mean temperature; EC_a is apparent electrical conductivity. The initial letter (w or d) refers to the temporal scale as weekly or daily, respectively, before the measurement of stem water potential. (**Left**): predictor variables that use TCARI as a core input. (**Right**): predictor variables that use ExG as a core input.

3.4. Regression of Grapevine Water Status Based on Core and Ancillary Variables

To test the potential usage of including the ancillary variables, core variables (i.e., TCARI or ExG) and different combinations of the ancillary variables composed the inputs for regression against Ψstem using EN, RFR, or SVR. The core variable must always be a modeling component. Ancillary variables were formed by one variable per cluster generated by hierarchical clustering, while the joining of variables from each cluster was optional. The total number of combinations tested was 576 (8 clusters: $3 \times 2 \times 3 \times 4 \times 1 \times 2 \times 2 \times 2$).

Compared to regression using VI only, there is a significant improvement in RMSE when including ancillary variables as inputs (Table 3, the first rows in Tables 5 and 6). RMSE is improved from 213 to 146 kPa for the TCARI-based model, while RMSE is improved from 221 to 138 kPa for the ExG-based model. In both models, SVR, a non-linear algorithm, was chosen to be the best descriptor for the relationship between Ψstem and the predictors. The scatter plots for both TCARI-based and ExG-based SVR models are presented in Figure 7.

From the second to the seventh rows in Tables 5 and 6, the modeling performance is presented to further assess the importance of ancillary variables in terms of their type (temporal, soil/terrain, and weather). According to the types of inputs used, only the machine learning model with the best predictive performance among the three machine learning models, in terms of RMSE on the test set, is presented. For both TCARI-based and ExG-based models, those used soil/terrain and temporal variables as inputs to capture the most variance. In terms of one type of ancillary predictor, models using terrain/soil variables as inputs have the worst performance for both TCARI-based and ExG-based models.

Table 5. Regression modeling using TCARI as core input along with different types of ancillary variables. RMSE is root mean square error, and RPIQ is ratio of performance to interquartile range.

Variable Composition	Machine Learning Algorithm	RMSE of the Train Set (kPa)	RPIQ of the Train Set	RMSE of the Test Set (kPa)	RPIQ of the Test Set
TCARI + full set of predictors	Support vector regression	139	3.02	146	2.60
TCARI + soil/terrain + weather	Random forest regression	159	2.64	163	2.33
TCARI + soil/terrain + temporal	Support vector regression	139	3.02	146	2.60
TCARI + weather + temporal	Random forest regression	149	2.81	153	2.48
TCARI + soil/terrain	Random forest regression	165	2.54	172	2.21
TCARI + temporal	Random forest regression	149	2.81	150	2.53
TCARI + weather	Random forest regression	158	2.65	163	2.33

Table 6. Regression modeling using ExG as core input along with different types of ancillary variables. RMSE is root mean square error, and RPIQ is ratio of performance to interquartile range.

Variable Composition	Machine Learning Algorithm	RMSE of the Train Set (kPa)	RPIQ of the Train Set	RMSE of the Test Set (kPa)	RPIQ of the Test Set
ExG + full set of predictors	Support vector regression	134	3.14	138	2.75
ExG + soil/terrain + weather	Random forest regression	139	3.02	142	2.66
ExG + soil/terrain + temporal	Support vector regression	135	3.10	141	2.69
ExG + weather + temporal	Support vector regression	138	3.03	143	2.65
ExG + soil/terrain	Random forest regression	196	2.14	214	1.77
ExG + temporal	Random forest regression	128	3.27	159	2.39
ExG + weather	Random forest regression	138	3.04	144	2.64

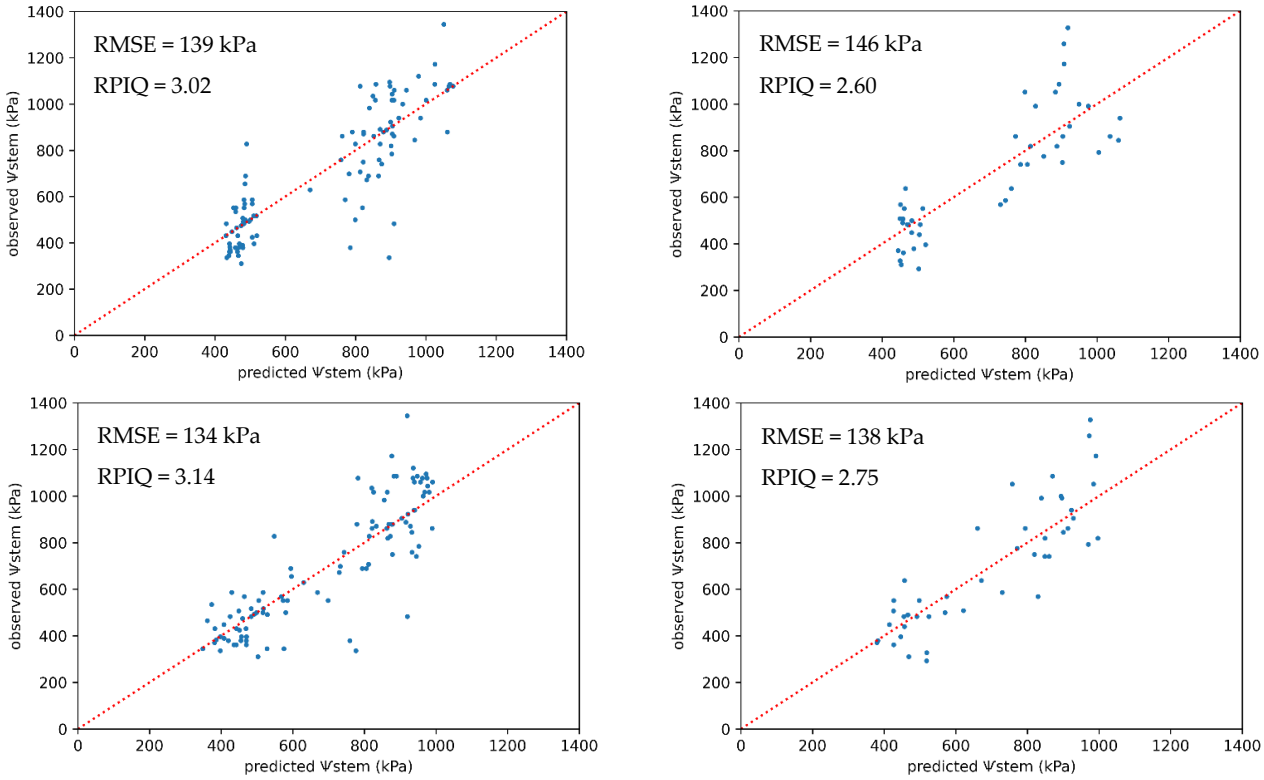

Figure 7. Scatter plots between predicted stem water potential and observed water potential for TCARI-based training set (**upper left**), TCARI-based test set (**upper right**), ExG-based training set (**lower left**), and ExG-based test set (**lower right**) using support vector regression based on the full set of predictors.

In terms of selected machine learning algorithms, both RFR and SVR are good descriptors to capture the variance of Ψstem when regressed against two types of ancillary variables (the second to fourth rows in Tables 5 and 6). RFR performs the best, shown by the fifth to seventh rows in Tables 5 and 6, for models based on one type of ancillary predictor, and the results of both SVR and EN are not presented because only the models with the best performance, in terms of RMSE on the test set, are displayed based on the types of inputs used.

3.5. Interpreting Models Using Shapley Additive exPlanations Analysis

To explore the impact of each predictor variable on modeling output and variation in Ψstem, SHAP was deployed to support the interpretability of machine learning models. The SHAP values indicate the contribution of the variable towards model prediction. For

Tables 5 and 6, the causal effects between Ψstem and predictor variables were assessed using SHAP, and only those models with reasonable relationships were selected and presented.

Only models based on full types of predictors in Tables 5 and 6 were analyzed and presented using SHAP analysis. In the summary plots of Figures 8 and 9, every point from each predictor refers to an observation. A wider spread of points along the axis of SHAP values indicates the variable has more influence on the output, thus being of more importance. The color of the points denotes the value of the variable for the observation, where red and blue colors refer to the high and low variable values, respectively. The summary plot shows how each variable influences the model prediction. For example, a red point with a negative SHAP value indicates that a higher value of the variable will have a negative contribution to the Ψstem value, the canopy becoming more hydrated. The bar plots of Figures 8 and 9 provide an overview of variable importance for each model. Both TCARI and ExG exhibit higher values when the grapevines are more hydrated. For the ExG-based model, it shows that higher wind speed leads grapevines to become more hydrated. The potential reasons underlying these relationships will be discussed in the next section.

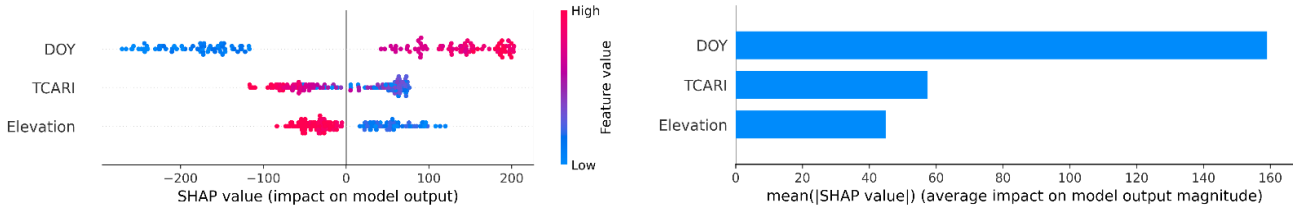

Figure 8. (**Left**): summary plot for regression modeling using TCARI and selected ancillary variables as inputs. (**Right**): bar plot for the predictor variables according to SHAP values received. Variables are ranked from top to bottom in descending order of average SHAP value, where DOY is day of the year; TCARI is transformed chlorophyll absorption reflectance index.

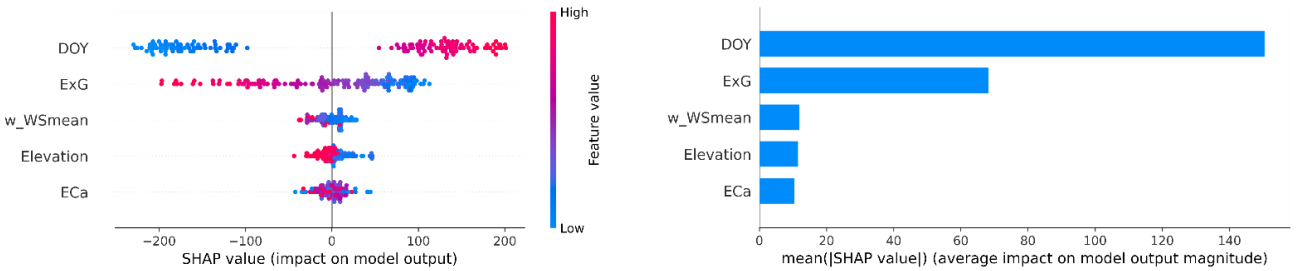

Figure 9. (**Left**): summary plot for regression modeling using ExG and selected ancillary variables as inputs. (**Right**): bar plot for the predictor variables according to SHAP values received. Variables are ranked from top to bottom in descending order of average SHAP value, where DOY is day of the year; ExG is excess green index; w_WSmean is weekly mean wind speed; EC_a is apparent electrical conductivity.

4. Discussion

4.1. Vegetation Indices and Stem Water Potential

Under water deficit, plants employ several adaptive strategies at leaf level, such as changes in leaf pigments and canopy structure, resulting in leaf curls and abscission [56–58]. These pigment and structural changes cause variation in multispectral reflectance, including the blue, green, red, red edge, and near-infrared (NIR) bands. Multispectral reflectance detects water status indirectly via reflectance changes in response to physiological and morphological variability as a consequence of water stress [59]. The blue band is characterized by the absorption of chlorophyll and carotenoids, which can be used as an indicator of the resistance of plants to stress, such as water deficit [60,61]. The energy in the green band is associated with the absorption by anthocyanins and reflection by chlorophyll [62]. The red band has been reported to be associated with the concentration of chlorophyll [63].

The reflectance and position of the red edge band, a transition region between red and NIR bands, has been proven to be sensitive to chlorophyll content in leaves [64,65]. The variation level of leaf water content alters cell turgidity and changes cell structure, which subsequently influences the absorption and reflection in the NIR band [66]. When crops experience water deficit, leaf chlorophyll content usually reduces, leading to a decrease in green reflection and an increase in blue and red reflection [67]. In addition, there is an increase in the concentration of de-epoxidized components of xanthophyll [56], while the alteration of canopy geometry results in a decrease in NIR reflection [68]. These basic characteristics lay the foundation for the use of vegetation indices (VIs) acquired from multispectral drones to monitor crop hydration status, as most of the current UAV systems do not include shortwave infrared bands [69].

Most of the variability of GWS in this study lies in non-stressed (Ψstem $\leq$ 800 kPa) and moderately stressed (800 kPa $\leq$ Ψstem $\leq$ 1200 kPa) ranges, while only three observations belong to the severely stressed range (Ψstem $\geq$ 1200 kPa) [23]. Using single multispectral VI, the capability of capturing the variance in GWS is poor, though the correlation is significant, with the best performance by TCARI, having an R^2 of 0.35 (Table 3). This unsatisfactory result is similar to that reported by Romero et al. [70], in which the best performance of all VIs was an R^2 of 0.42. A possible explanation for this may be related to the sensitivity of canopy structure and leaf pigments to various levels of water stress for different crop species [63]. For example, chlorophyll is affected after severe dehydration treatment or after an extended period of water deficit [71], so VIs associated with chlorophyll variation may not be sensitive enough to detect mild water stress or short-term dehydration. Moreover, a study has shown that differences in spectral resolution could influence values of VIs, such as NDVI [72], which can compromise the relationship between spectral indices and the variable of interest.

According to Zhang et al. [73], multispectral VIs related to water deficit can be classified as chlorophyll and structural VIs based on their sensitivity to changes in physiological or morphological characteristics. Chlorophyll VIs are derived from blue, green, red, or red edge bands, so they are more sensitive to changes in chlorophyll concentration. TCARI, ExG, and TCARI/OSAVI belong to this category. Structural VIs are computed based on spectral bands, including NIR, so they are both influenced by chlorophyll and leaf scattering caused by changes in plant structure and involve the use of GNDVI, NDRE, and NDVI. It is interesting to note that chlorophyll VIs are very good at capturing the variance of Ψstem (Table 3). This implies that the water stress level of the grapevine used in this study, Pinot Noir, is described better via observation of chlorophyll-related VIs compared to structure-related VIs. Research carried out at Pinot Noir vineyards in New Zealand over two growing seasons [74] stated that dehydration treatment did not have an overall effect on the reduction of leaf area and that this effect started becoming evident from veraison onwards. They highlighted the usefulness of using chlorophyll content in water stress studies, which supports our results. The top five VIs (TCARI, ExG, TCARI/OSAVI, GNDVI, NDRE, and one frequently used VI, NDVI), in terms of its R^2, are the focus for the following discussion.

Among the chlorophyll VIs, TCARI (R^2 = 0.35) explains more variance in GWS than ExG (R^2 = 0.3) does in terms of their correlation coefficients, followed by TCARI/OSAVI (R^2 = 0.24). TCARI is a VI, which is sensitive to chlorophyll concentration, while TCARI/OSAVI has been proposed to minimize the effects posed by soil reflectance and changes in leaf area index (LAI) [35]. The better performance of TCARI compared to the modified index (TCARI/OSAVI) may indicate that the LAI of grapevines was relatively stable and high, thus swamping any noise from the soil background during the study period. This finding is supported by the study of Baluja et al. [75], in which TCARI (R^2 = 0.45) and TCARI/OSAVI (R^2 = 0.58) were significantly correlated with the Ψstem of rain-fed Tempranillo grapevines in Spain. TCARI yields a better correlation with Ψstem than ExG, probably due to the inclusion of the red edge band. This behavior was also observed at Petite Sirah and Cabernet Sauvignon vineyards in California, USA [28]. ExG is a VI highlighting a green band to

separate vegetation from the background, and thus is sensitive to canopy greenness [36]. A good correlation between ExG and GWS was also found to be evident for grapevines faced with different irrigation treatments at a Vermentino vineyard in Italy [76]. The good performance of ExG suggests that it has the potential of detecting GWS using just RGB sensors instead of multispectral sensors. This may increase the applicability of UAV-based imagery because RGB cameras do not require an extra filter and post-processing work to generate NIR readings, thus reducing the cost of sensors [77].

Both GNDVI and NDRE have been reported to be sensitive to variations in chlorophyll concentration [38,78]. Due to the modification of chlorophyll content under water stress, GNDVI was observed to be able to differentiate Cabernet Sauvignon grapevines between the moderate and severe classes of water deficit [79]. A good correlation between GNDVI and Ψstem was recorded by Baluja et al. [75] and Poblete et al. for Carménère grapevines planted in Chile [59], in which R^2 was 0.58 and 0.31, respectively. NDRE was observed to outperform other multispectral indices when correlated with leaf water potential, with a Pearson correlation coefficient of −0.27 [28]. NDVI is the most used VI in agriculture, as it is related to plant biomass, vigor, and health. In viticulture, the growth of shoots is inhibited after experiencing water deficit [80], and that development state, quantified by pruning weight and LAI, has been shown to be strongly related to NDVI [81]. Acevedo-Opazo et al. [23] have observed a significant difference in pre-dawn leaf water potential between high and low NDVI zones for seven cultivars grown in France. However, in this study, the correlation between NDVI and Ψstem is weak (R^2 = 0.04). The poor performance of NDVI is supported by Romero et al. [70], whose research indicated that the red and NIR bands could be used as long-term predictors of water deficit as correlation improved over the season. Another explanation is the saturation effect of NDVI values, which usually happens when applied to very dense canopies. In the research of Junges et al. [82], a lower standard deviation of 0.01 was calculated when NDVI was measured close to 0.8 for Cabernet Sauvignon grapevines planted in Brazil. This value is similar to this study's NDVI recordings (average = 0.74; maximum = 0.82; standard deviation = 0.06).

4.2. Important Ancillary Variables: Day of the Year, Elevation, Electrical Conductivity, and Wind Speed

Inspired by the concept of a soil-plant-atmosphere continuum for water movement in nature [83], various ancillary estimators (other than VIs) have been used to help describe the dynamics of GWS (Table 4). Plant water status during the day is a consequence of water uptake (mainly dependent on characteristics of the root system and soil moisture), as well as transpiration (mainly dependent on a number of atmospheric variables and stomatal conductance) [84]. In this study, it was assumed that Ψstem was more strongly associated with soil water status and weather conditions. This assumption was made because the cultivar effect has been removed, as only Pinot Noir with similar canopy ages were examined. In addition, daylight is assumed to be the main driver to stomatal opening in this study. As the temperature is mild and rainfall is moderate in Martinborough, the occurrence of additional processes such as stomatal closure induced by abscisic acid resulting from soil water deficit may be reduced. Moreover, Pinot Noir is considered to be a near-anisohydric cultivar, so its control on stomata is less responsive to decreases in soil moisture [85].

The selected core VIs (TCARI and ExG) exhibiting chlorophyll variability are the variables representing the mid-term impact imposed by water deficit, as the chlorophyll content changes in accordance with the level of dehydration during the growing period. It is assumed that the predictive capacities for Ψstem can be significantly improved when complementing VIs with comparable long-term and short-term variables. Soil/terrain variables represent long-term effects, as they consistently affect GWS over years [86]. The temporal variable is relatively mid- to short-term because it reflects the time trend along the growing season. Weekly or daily weather variables are short term. The complementary effects among different types of variables are reflected in Tables 5 and 6. When using two

types of ancillary predictors, the composition of predictors (VI, soil/terrain, and temporal variables) captures the most variance in Ψstem in both TCARI-based and ExG-based models. When using solely one type of ancillary predictor, the combination of VI and temporal or weather variables produces models with the best performance, similar to the performance of the models using two types of ancillary predictors. This indicates that using variables with mid- to short-term effects may be sufficient to describe the variation of Ψstem in this study. TCARI and ExG-based models had the worst performance when combined with soil/terrain variables, while the ExG-based model performed worse than the TCARI-based model. This may be because the ExG captures relatively mid to long-term effects of water stress on chlorophyll content, while TCARI captures relatively short to mid-term effects. This supports the result when using a full set of ancillary predictors (Figures 8 and 9). The best performing TCARI-based model does not select any weather variables, and the ExG-based model selects one weather variable as an input.

The summary plots in Figures 8 and 9 provide insights into the relationships between Ψstem and the selected ancillary variables (DOY), elevation, EC_a, and weekly mean wind speed). DOY represents seasonality along the growing season. DOY positively contributes to the dehydration of the grapevine (Figures 8 and 9). Irrigation was only applied at the end of the study periods in the first growing season, with heavy precipitation concentrated around flowering and fruit set and subsequent gentle (<10 mm) rainfall (Figure 2). As a result, there is a downward trend of Ψstem (increasing hydration) from late November to late January (Figure 5) in accordance with the increase in DOY. In the study of Suter et al. [27], DOY explained a great part of the variability in the Ψstem of three cultivars grown in France.

SHAP summary plots show that grapevines are more hydrated when they stand on more elevated ground. It is contrary to the concept in which water accumulation happens in the lower parts of fields so that crops would stay at high hydration levels. When evaluating terrain information of observations at both vineyards, Pencarrow, ranging between 44–46 m elevation, is higher than Wharekauhau, ranging between 36–38 m. The recorded elevation of observations from Wharekauhau is significantly lower than that of observations from Pencarrow (p-value of Mann-Whitney U test is lower than 0.05). One explanation is that the higher landscape terraces, older than 15K years, are likely to have a covering of loess. Loess is a well-sorted quartzo-feldspathic material of silt to clay-sized particles, and it is picked up by wind from nearby aggrading braided riverbeds present during historic global cold cycles. This fine loess will increase the water holding capacity of the soils developing on these higher and older terraces. Loess deposition will not be present on lower terraces with an age younger than 15K years, where the soils are much more likely to be developing from alluvial deposits from consecutive flooding events over the last 15K years. These deposits have a potentially wider range of textures from silt to sand and coarse sand. The soils developing from them are likely to be better drained. The soil properties were reported to affect soil water holding capacity, further leading to spatial differences in GWS across the fields [26]. Thus, Pencarrow, sited on the higher terrace, may have the ability to hold more water than Wharekauhau due to differences in particle composition, enabling grapevines to be more hydrated.

EC_a was selected as an important predictor for the ExG-based model. EC_a has been demonstrated to be related to spatial changes in GWS (R^2 = 0.56) due to its association with differences in soil water availability [87]. The contribution of EC to Ψstem (Figure 9) does not follow a regular pattern. Higher clay content usually leads to higher EC_a because clay particles can adsorb more water [88]. However, the EC_a survey in this study was taken during a wet period, and soil EC_a recorded in this kind of period was influenced by both soil moisture content and clay content [89]. Therefore, the relationship between EC_a and Ψstem is not straightforward. Other sources of variation include the spatial sensitivity of the EM38 instrument [90], the size of the root ball of each canopy, and the physical properties of the soils hosting the functional roots. These factors will determine how precisely EC_a values represent the soil properties influencing each grapevine.

Of the weather variables, only weekly mean wind speed (mean = 1.5 m/s, standard deviation = 0.6 m/s, and maximum = 3 m/s) was selected by the ExG-based model (Figure 9). Crop transpiration is influenced by weather through the effects on the driving force, including vapor pressure deficit (VPD) and the resistance, including stomatal resistance (r_s) and boundary layer resistance (r_b). VPD is a function of temperature, which depends on solar radiation and relative humidity. Solar radiation, temperature, and wind speed impact r_s and r_b, with wind speed dominating [91]. In the summary plots (Figures 8 and 9), it is interesting to note that there is a general trend of negative response of grapevine dehydration to windspeed, as blue points positively contribute to Ψstem. This is contradictory to the general understanding in which water stress is induced by both increasing evapotranspiration demands and decreasing boundary layers, both resulting from high wind speed [92]. These results are supported by several studies that have observed grapevines reducing transpiration, via partial closure of stomata, to prevent water loss. Two studies measured this phenomenon when wind speeds are higher than 3.6 m/s for six cultivars grown in pots [93] and 4 m/s for two cultivars planted in Western Australia [94]. An additional reason could be more efficient convective cooling, resulting from a thinner boundary layer or high humidity of the air circulating around leaves, removing heat from the irradiated leaf surface, rather than relying on evaporative cooling [95]. Temperature, irradiance, humidity, and rainfall are widely accepted as important weather factors influencing the variation in Ψstem. The reason those variables were not selected in our models was due to the length of the study window. In this study, the two months between flowering to veraison were selected due to their significance to GWS monitoring. This may not be sufficient to sample broader variability in these weather variables.

4.3. Regression Modeling

The relationship between Ψstem and soil/terrain, temporal, and weather variables is complex, so machine learning algorithms, including EN, RFR, and SVR, were utilized to describe the relationship. As R^2 is an inadequate measure for nonlinear models [96], it was not used in evaluating modeling performance. According to the results listed in Tables 5 and 6, the relationship seems to be non-linear, since EN is a linear regression model with penalty terms and does not outperform RFR or SVR when using any set of predictors. When modeling is based on all types of predictors, SVR has the best performance in both TCARI-based and ExG-based models. When based on two types of predictors, either SVR or RFR is selected as the best descriptor. When only one type of predictor is used in regression, RFR outperforms the other algorithms. It appears SVR is capable of handling more variables, especially when soil/terrain and temporal variables are included in simulating changes in Ψstem. One explanation is that this dataset may be limited (n = 148) and have appreciable noise. However, SVR has been reported to be less sensitive to sampling variation for a small sample size because the selection of support vectors depends on only a small subset of observations [55,97]. Moreover, the close values between RMSE for training and test sets show the overfitting issue in our models was addressed well. This indicates that the range of the regularized hyperparameters (the maximum depth of the tree for RFR, regularization parameter, and width of the epsilon-tube for SVR) are set correctly for the study. Interpretation of the results supports using SVR for remote monitoring of Pinot Noir Ψstem if the regression is based on terrain/soil, temporal, and weather variables, but more machine learning algorithms need to be investigated to optimize the estimation performance.

4.4. Limitations and Future Work

By combining UAV-based multispectral imagery with ancillary variables, the approach presented in this study demonstrates the potential usefulness of using UAVs to estimate GWS at canopy scale across the vineyard when the locations of perennial grapevines in a vineyard are precisely marked. However, this study uses an empirical approach, so it does not fully describe the relationships between soil/terrain, weather, spectral information,

and grapevine water status. As summarized by Adams et al. [98], empirical approaches are highly dependent on the range and the quality of inputs and can yield significant bias when used to extrapolate identified relationships beyond observed variability. The methodology demonstrated in this study could serve as a useful tool under the following conditions: the training datasets incorporate a rich variation in high-quality values of predictors corresponding to a range of sites, environmental conditions, grapevine cultivars, growing stages, canopy ages, and management practices. Machine learning modeling is undertaken with extensive calibration. Additional variables, such as soil moisture, can be investigated for their usefulness as ancillary variables. To enhance the modeling performance and transferability, it will be necessary to enlarge the input datasets. This is a time-consuming process, involving the collection of a large number of Ψstem measurements by pressure bomb within the two hours of midday. This will require considerable manpower and calibrated pressure bombs. Once these conditions are met, the model developed in this study may be applied to other vineyards, cultivars, or, perhaps, regional scale analysis.

5. Conclusions

This study explores the potential of combining UAV-based vegetation indices (VIs) and various ancillary data (soil/terrain, temporal, and weather variables) for the estimation of stem water potential (Ψstem), used as a proxy for grapevine water status (GWS). It uses machine learning algorithms and SHAP analysis, based on observations collected in two Pinot Noir vineyards in New Zealand, over two growing seasons. The results demonstrate the potential and the techniques associated with developing a useful tool for GWS monitoring by taking advantage of the complementary effects between vegetation, soil/terrain, weather, and temporal variables. SHAP analysis facilitates the interpretability of the GWS model, which could be useful for GWS manipulation. A broader range of predictor values is needed to train and calibrate the models for enhancing the transferability of GWS models to other vineyards. In addition, it is recommended that new machine learning algorithms be investigated to optimize the performance of Ψstem estimation. For viticulturists and growers, the tool developed in this study could enable precise scheduling of irrigation for quality management from canopy to sub-block scale in response to the types of irrigation equipment available.

Author Contributions: H.-E.W. undertook this research as part of his Ph.D. Conceptualization, H.-E.W., M.G., M.B. and M.I.; methodology, H.-E.W., M.G., M.B. and M.I.; validation, H.-E.W.; formal analysis, H.-E.W.; investigation, H.-E.W., M.I. and E.S.; resources, M.I. and E.S.; writing—original draft preparation, H.-E.W.; writing—review and editing, M.G. and M.B.; visualization, H.-E.W. and M.I.; supervision, M.G., M.B. and M.I. All authors have read and agreed to the published version of the manuscript.

Funding: This study was funded by a grant from the 2020 Massey University Research Fund (MURF) and a grant from the New Zealand Horticulture Trust.

Data Availability Statement: Not applicable.

Acknowledgments: The authors sincerely thank Palliser Estate for providing the vineyards as study fields, as well as Guy McMaster (chief viticulturist of Palliser Estate) for offering the pressure chamber during the research period. Additional thanks are given to the New Zealand eScience Infrastructure (NeSI) for providing the platform of high performance computing for the use of modeling and data analysis.

Conflicts of Interest: The authors declare no conflict of interest.

References

1. Ojeda, H.; Andary, C.; Kraeva, E.; Carbonneau, A.; Deloire, A. Influence of pre-and postveraison water deficit on synthesis and concentration of skin phenolic compounds during berry growth of *Vitis vinifera* cv. Shiraz. *Am. J. Enol. Vitic.* **2002**, *53*, 261–267.
2. Martínez-Lüscher, J.; Sánchez-Díaz, M.; Delrot, S.; Aguirreolea, J.; Pascual, I.; Gomes, E. Ultraviolet-B Radiation and Water Deficit Interact to Alter Flavonol and Anthocyanin Profiles in Grapevine Berries through Transcriptomic Regulation. *Plant Cell Physiol.* **2014**, *55*, 1925–1936. [CrossRef] [PubMed]

3. Van Leeuwen, C.; Trégoat, O.; Choné, X.; Bois, B.; Pernet, D.; Gaudillère, J.-P. Vine water status is a key factor in grape ripening and vintage quality for red Bordeaux wine. How can it be assessed for vineyard management purposes? *J. Int. Sci. Vigne Vin* **2009**, *43*, 121–134. [CrossRef]
4. Acevedo-Opazo, C.; Valdés-Gómez, H.; Taylor, J.; Avalo, A.; Verdugo-Vásquez, N.; Araya, M.; Jara-Rojas, F.; Tisseyre, B. Assessment of an empirical spatial prediction model of vine water status for irrigation management in a grapevine field. *Agric. Water Manag.* **2013**, *124*, 58–68. [CrossRef]
5. Intrigliolo, D.S.; Castel, J.R. Response of grapevine cv. 'Tempranillo' to timing and amount of irrigation: Water relations, vine growth, yield and berry and wine composition. *Irrig. Sci.* **2009**, *28*, 113–125. [CrossRef]
6. Etchebarne, F.; Ojeda, H.; Hunter, J. Leaf: Fruit ratio and vine water status effects on Grenache Noir (*Vitis vinifera* L.) berry composition: Water, sugar, organic acids and cations. *S. Afr. J. Enol. Vitic.* **2010**, *31*, 106–115.
7. Min, Z.; Li, R.; Chen, L.; Zhang, Y.; Li, Z.; Liu, M.; Ju, Y.; Fang, Y. Alleviation of drought stress in grapevine by foliar-applied strigolactones. *Plant Physiol. Biochem.* **2019**, *135*, 99–110. [CrossRef]
8. Brillante, L.; Martínez-Luscher, J.; Yu, R.; Plank, C.M.; Sanchez, L.; Bates, T.L.; Brenneman, C.; Oberholster, A.; Kurtural, S.K. Assessing Spatial Variability of Grape Skin Flavonoids at the Vineyard Scale Based on Plant Water Status Mapping. *J. Agric. Food Chem.* **2017**, *65*, 5255–5265. [CrossRef]
9. López-García, P.; Intrigliolo, D.S.; Moreno, M.A.; Martínez-Moreno, A.; Ortega, J.F.; Pérez-Álvarez, E.P.; Ballesteros, R. Assessment of Vineyard Water Status by Multispectral and RGB Imagery Obtained from an Unmanned Aerial Vehicle. *Am. J. Enol. Vitic.* **2021**, *72*, 285–297. [CrossRef]
10. Bramley, R.; Ouzman, J.; Boss, P. Variation in vine vigour, grape yield and vineyard soils and topography as indicators of variation in the chemical composition of grapes, wine and wine sensory attributes. *Aust. J. Grape Wine Res.* **2011**, *17*, 217–229. [CrossRef]
11. Baciocco, K.A.; Davis, R.E.; Jones, G.V. Climate and Bordeaux wine quality: Identifying the key factors that differentiate vintages based on Consensus rankings. *J. Wine Res.* **2014**, *25*, 75–90. [CrossRef]
12. Liu, C.; Sun, P.-S.; Liu, S.-R. A review of plant spectral reflectance response to water physiological changes. *Chin. J. Plant Ecol.* **2016**, *40*, 80.
13. Bowyer, P.; Danson, F. Sensitivity of spectral reflectance to variation in live fuel moisture content at leaf and canopy level. *Remote Sens. Environ.* **2004**, *92*, 297–308. [CrossRef]
14. Jang, G.; Kim, J.; Yu, J.-K.; Kim, H.-J.; Kim, Y.; Kim, D.-W.; Kim, K.-H.; Lee, C.W.; Chung, Y.S. Review: Cost-Effective Unmanned Aerial Vehicle (UAV) Platform for Field Plant Breeding Application. *Remote Sens.* **2020**, *12*, 998. [CrossRef]
15. Rapaport, T.; Hochberg, U.; Shoshany, M.; Karnieli, A.; Rachmilevitch, S. Combining leaf physiology, hyperspectral imaging and partial least squares-regression (PLS-R) for grapevine water status assessment. *ISPRS J. Photogramm. Remote Sens.* **2015**, *109*, 88–97. [CrossRef]
16. Brook, A.; De Micco, V.; Battipaglia, G.; Erbaggio, A.; Ludeno, G.; Catapano, I.; Bonfante, A. A smart multiple spatial and temporal resolution system to support precision agriculture from satellite images: Proof of concept on Aglianico vineyard. *Remote Sens. Environ.* **2020**, *240*, 111679. [CrossRef]
17. Arevalo-Ramirez, T.; Villacrés, J.; Fuentes, A.; Reszka, P.; Cheein, F.A.A. Moisture content estimation of Pinus radiata and Eucalyptus globulus from reconstructed leaf reflectance in the SWIR region. *Biosyst. Eng.* **2020**, *193*, 187–205. [CrossRef]
18. Jenal, A.; Bareth, G.; Bolten, A.; Kneer, C.; Weber, I.; Bongartz, J. Development of a VNIR/SWIR Multispectral Imaging System for Vegetation Monitoring with Unmanned Aerial Vehicles. *Sensors* **2019**, *19*, 5507. [CrossRef]
19. Kandylakis, Z.; Falagas, A.; Karakizi, C.; Karantzalos, K. Water Stress Estimation in Vineyards from Aerial SWIR and Multispectral UAV Data. *Remote Sens.* **2020**, *12*, 2499. [CrossRef]
20. Choné, X.; Van Leeuwen, C.; Dubourdieu, D.; Gaudillère, J.P. Stem Water Potential is a Sensitive Indicator of Grapevine Water Status. *Ann. Bot.* **2001**, *87*, 477–483. [CrossRef]
21. Taylor, J.; Acevedo-Opazo, C.; Ojeda, H.; Tisseyre, B. Identification and significance of sources of spatial variation in grapevine water status. *Aust. J. Grape Wine Res.* **2010**, *16*, 218–226. [CrossRef]
22. Irmak, S.; Mutiibwa, D. On the dynamics of canopy resistance: Generalized linear estimation and relationships with primary micrometeorological variables. *Water Resour. Res.* **2010**, *46*. [CrossRef]
23. Acevedo-Opazo, C.; Tisseyre, B.; Guillaume, S.; Ojeda, H. The potential of high spatial resolution information to define within-vineyard zones related to vine water status. *Precis. Agric.* **2008**, *9*, 285–302. [CrossRef]
24. Acevedo-Opazo, C.; Tisseyre, B.; Taylor, J.A.; Ojeda, H.; Guillaume, S. A model for the spatial prediction of water status in vines (*Vitis vinifera* L.) using high resolution ancillary information. *Precis. Agric.* **2010**, *11*, 358–378. [CrossRef]
25. Taylor, J.A.; Acevedo-Opazo, C.; Pellegrino, A.; Ojeda, H.; Tisseyre, B. Can within-season grapevine predawn leaf water potentials be predicted from meteorological data in non-irrigated Mediterranean vineyards? *OENO One* **2012**, *46*, 221–232. [CrossRef]
26. Brillante, L.; Mathieu, O.; Lévêque, J.; Bois, B. Ecophysiological Modeling of Grapevine Water Stress in Burgundy Terroirs by a Machine-Learning Approach. *Front. Plant Sci.* **2016**, *7*, 796. [CrossRef]
27. Suter, B.; Triolo, R.; Pernet, D.; Dai, Z.; Van Leeuwen, C. Modeling Stem Water Potential by Separating the Effects of Soil Water Availability and Climatic Conditions on Water Status in Grapevine (*Vitis vinifera* L.). *Front. Plant Sci.* **2019**, *10*, 1485. [CrossRef]
28. Tang, Z.; Jin, Y.; Alsina, M.M.; McElrone, A.J.; Bambach, N.; Kustas, W.P. Vine water status mapping with multispectral UAV imagery and machine learning. *Irrig. Sci.* **2022**, *40*, 715–730. [CrossRef]

29. Kuhn, M.; Johnson, K. Data pre-processing. In *Applied Predictive Modeling*; Springer Science Business Media: New York, NY, USA, 2013; pp. 27–59.
30. Lundberg, S.M.; Lee, S.-I. A unified approach to interpreting model predictions. In Proceedings of the 31st International Conference on Neural Information Processing Systems, Long Beach, CA, USA, 4–9 December 2017.
31. Lundberg, S.M.; Erion, G.; Chen, H.; DeGrave, A.; Prutkin, J.M.; Nair, B.; Katz, R.; Himmelfarb, J.; Bansal, N.; Lee, S.-I. From local explanations to global understanding with explainable AI for trees. *Nat. Mach. Intell.* **2020**, *2*, 56–67. [CrossRef]
32. Mangalathu, S.; Hwang, S.-H.; Jeon, J.-S. Failure mode and effects analysis of RC members based on machine-learning-based SHapley Additive exPlanations (SHAP) approach. *Eng. Struct.* **2020**, *219*, 110927. [CrossRef]
33. Patakas, A.; Noitsakis, B.; Chouzouri, A. Optimization of irrigation water use in grapevines using the relationship between transpiration and plant water status. *Agric. Ecosyst. Environ.* **2005**, *106*, 253–259. [CrossRef]
34. Giovos, R.; Tassopoulos, D.; Kalivas, D.; Lougkos, N.; Priovolou, A. Remote Sensing Vegetation Indices in Viticulture: A Critical Review. *Agriculture* **2021**, *11*, 457. [CrossRef]
35. Haboudane, D.; Miller, J.R.; Tremblay, N.; Zarco-Tejada, P.J.; Dextraze, L. Integrated narrow-band vegetation indices for prediction of crop chlorophyll content for application to precision agriculture. *Remote Sens. Environ.* **2002**, *81*, 416–426. [CrossRef]
36. Woebbecke, D.M.; Meyer, G.E.; Von Bargen, K.; Mortensen, D.A. Color Indices for Weed Identification Under Various Soil, Residue, and Lighting Conditions. *Trans. ASAE* **1995**, *38*, 259–269. [CrossRef]
37. Barnes, E.M.; Clarke, T.R.; Richards, S.E.; Colaizzi, P.D.; Haberland, J.; Kostrzewski, M.; Waller, P.; Choi, C.; Riley, E.; Thompson, T.; et al. Coincident detection of crop water stress, nitrogen status and canopy density using ground based multispectral data. In Proceedings of the Fifth International Conference on Precision Agriculture, Bloomington, MN, USA, 16–19 July 2000.
38. Gitelson, A.A.; Merzlyak, M.N. Remote sensing of chlorophyll concentration in higher plant leaves. *Adv. Space Res.* **1998**, *22*, 689–692. [CrossRef]
39. Gitelson, A.A.; Viña, A.; Ciganda, V.; Rundquist, D.C.; Arkebauer, T.J. Remote estimation of canopy chlorophyll content in crops. *Geophys. Res. Lett.* **2005**, *32*, L08403. [CrossRef]
40. Haboudane, D.; Miller, J.R.; Pattey, E.; Zarco-Tejada, P.J.; Strachan, I.B. Hyperspectral vegetation indices and novel algorithms for predicting green LAI of crop canopies: Modeling and validation in the context of precision agriculture. *Remote Sens. Environ.* **2004**, *90*, 337–352. [CrossRef]
41. Huete, A.; Didan, K.; Miura, T.; Rodriguez, E.P.; Gao, X.; Ferreira, L.G. Overview of the radiometric and biophysical performance of the MODIS vegetation indices. *Remote Sens. Environ.* **2002**, *83*, 195–213. [CrossRef]
42. Tucker, C.J. Red and photographic infrared linear combinations for monitoring vegetation. *Remote Sens. Environ.* **1979**, *8*, 127–150. [CrossRef]
43. Qi, J.; Chehbouni, A.; Huete, A.R.; Kerr, Y.H.; Sorooshian, S. A modified soil adjusted vegetation index. *Remote Sens. Environ.* **1994**, *48*, 119–126. [CrossRef]
44. Birth, G.S.; McVey, G.R. Measuring the Color of Growing Turf with a Reflectance Spectrophotometer. *Agron. J.* **1968**, *60*, 640–643. [CrossRef]
45. Rouse, J.W.; Haas, R.H.; Schell, J.A.; Deering, D.W.; Harlan, J.C. *Monitoring the Vernal Advancements and Retrogradation*; Texas A & M University: College Station, TX, USA, 1974.
46. Rondeaux, G.; Steven, M.; Baret, F. Optimization of soil-adjusted vegetation indices. *Remote Sens. Environ.* **1996**, *55*, 95–107. [CrossRef]
47. Gamon, J.A.; Surfus, J.S. Assessing leaf pigment content and activity with a reflectometer. *New Phytol.* **1999**, *143*, 105–117. [CrossRef]
48. Gitelson, A.A.; Kaufman, Y.J.; Stark, R.; Rundquist, D. Novel algorithms for remote estimation of vegetation fraction. *Remote Sens. Environ.* **2002**, *80*, 76–87. [CrossRef]
49. Daughtry, C.S.T.; Walthall, C.L.; Kim, M.S.; De Colstoun, E.B.; McMurtrey, J.E., III. Estimating Corn Leaf Chlorophyll Concentration from Leaf and Canopy Reflectance. *Remote Sens. Environ.* **2000**, *74*, 229–239. [CrossRef]
50. Ballesteros, R.; Ortega, J.F.; Hernández, D.; Moreno, M. Characterization of *Vitis vinifera* L. Canopy Using Unmanned Aerial Vehicle-Based Remote Sensing and Photogrammetry Techniques. *Am. J. Enol. Vitic.* **2015**, *66*, 120–129. [CrossRef]
51. Cook, P.; Williams, B. *Electromagnetic Induction Techniques—Part 8*; CSIRO Publishing: Clayton, Australia, 1998. [CrossRef]
52. Heil, K.; Schmidhalter, U. The Application of EM38: Determination of Soil Parameters, Selection of Soil Sampling Points and Use in Agriculture and Archaeology. *Sensors* **2017**, *17*, 2540. [CrossRef]
53. Brevik, E.C.; Fenton, T.E.; Lazari, A. Soil electrical conductivity as a function of soil water content and implications for soil mapping. *Precis. Agric.* **2006**, *7*, 393–404. [CrossRef]
54. Morgenthaler, S. Exploratory data analysis. *Wiley Interdiscip. Rev. Comput. Stat.* **2009**, *1*, 33–44. [CrossRef]
55. James, G.; Witten, D.; Hastie, T.; Tibshirani, R. *An Introduction to Statistical Learning*; Springer: New York, NY, USA, 2013; Volume 112.
56. Chaves, M.M.; Pereira, J.S.; Marôco, J.; Rodrigues, M.L.; Ricardo, C.P.P.; Osório, M.L.; Carvalho, I.; Faria, T.; Pinheiro, C. How Plants Cope with Water Stress in the Field? Photosynthesis and Growth. *Ann. Bot.* **2002**, *89*, 907–916. [CrossRef]
57. Turner, N.; Begg, J.E. Plant-water relations and adaptation to stress. *Plant Soil* **1981**, *58*, 97–131. [CrossRef]
58. Ballester, C.; Brinkhoff, J.; Quayle, W.C.; Hornbuckle, J. Monitoring the Effects of Water Stress in Cotton Using the Green Red Vegetation Index and Red Edge Ratio. *Remote Sens.* **2019**, *11*, 873. [CrossRef]

59. Poblete, T.; Ortega-Farías, S.; Moreno, M.A.; Bardeen, M. Artificial Neural Network to Predict Vine Water Status Spatial Variability Using Multispectral Information Obtained from an Unmanned Aerial Vehicle (UAV). *Sensors* **2017**, *17*, 2488. [CrossRef]
60. Steele, M.R.; Gitelson, A.A.; Rundquist, D.C.; Merzlyak, M.N. Nondestructive Estimation of Anthocyanin Content in Grapevine Leaves. *Am. J. Enol. Vitic.* **2009**, *60*, 87–92. [CrossRef]
61. Gitelson, A. Nondestructive estimation of foliar pigment (chlorophylls, carotenoids and anthocyanins) contents: Evaluating a semianalytical three-band model. In *Hyperspectral Remote Sensing of Vegetation*; Thenkabail, P.S., Lyon, J.G., Eds.; CRC Press: Boca Raton, FL, USA, 2011; pp. 141–166.
62. Viña, A.; Gitelson, A.A.; Nguy-Robertson, A.L.; Peng, Y. Comparison of different vegetation indices for the remote assessment of green leaf area index of crops. *Remote Sens. Environ.* **2011**, *115*, 3468–3478. [CrossRef]
63. Ballester, C.; Zarco-Tejada, P.J.; Nicolás, E.; Alarcón, J.J.; Fereres, E.; Intrigliolo, D.S.; Gonzalez-Dugo, V. Evaluating the performance of xanthophyll, chlorophyll and structure-sensitive spectral indices to detect water stress in five fruit tree species. *Precis. Agric.* **2018**, *19*, 178–193. [CrossRef]
64. Clevers, J.; De Jong, S.; Epema, G.F.; Van Der Meer, F.D.; Bakker, W.H.; Skidmore, A.; Scholte, K.H. Derivation of the red edge index using the MERIS standard band setting. *Int. J. Remote Sens.* **2002**, *23*, 3169–3184. [CrossRef]
65. Campbell, P.K.E.; Middleton, E.M.; McMurtrey, J.E.; Corp, L.A.; Chappelle, E.W. Assessment of Vegetation Stress Using Reflectance or Fluorescence Measurements. *J. Environ. Qual.* **2007**, *36*, 832–845. [CrossRef] [PubMed]
66. Satterwhite, M.B.; Henley, J.P. *Hyperspectral Signatures (400 to 2500 nm) of Vegetation, Minerals, Soils, Rocks, and Cultural Features: Laboratory and Field Measurements*; Army Engineer Topographic Labs: Fort Belvoir, VA, USA, 1990.
67. Zarco-Tejada, P.J.; Miller, J.R.; Mohammed, G.H.; Noland, T.L. Chlorophyll fluorescence effects on vegetation apparent reflectance: I. Leaf-level measurements and model simulation. *Remote Sens. Environ.* **2000**, *74*, 582–595. [CrossRef]
68. Cogato, A.; Wu, L.; Jewan, S.Y.Y.; Meggio, F.; Marinello, F.; Sozzi, M.; Pagay, V. Evaluating the Spectral and Physiological Responses of Grapevines (*Vitis vinifera* L.) to Heat and Water Stresses under Different Vineyard Cooling and Irrigation Strategies. *Agronomy* **2021**, *11*, 1940. [CrossRef]
69. Maimaitijiang, M.; Sagan, V.; Sidike, P.; Daloye, A.M.; Erkbol, H.; Fritschi, F.B. Crop Monitoring Using Satellite/UAV Data Fusion and Machine Learning. *Remote Sens.* **2020**, *12*, 1357. [CrossRef]
70. Romero, M.; Luo, Y.; Su, B.; Fuentes, S. Vineyard water status estimation using multispectral imagery from an UAV platform and machine learning algorithms for irrigation scheduling management. *Comput. Electron. Agric.* **2018**, *147*, 109–117. [CrossRef]
71. Zulini, L.; Rubinigg, M.; Zorer, R.; Bertamini, M. Effects of Drought Stress on Chlorophyll Fluorescence and Photosynthetic Pigments in Grapevine Leaves (*Vitis vinifera* CV. 'White Riesling'). In *International Workshop on Advances in Grapevine and Wine Research 754*; Washington State University: Pullman, WA, USA, 2005. [CrossRef]
72. Teillet, P.; Staenz, K.; William, D. Effects of spectral, spatial, and radiometric characteristics on remote sensing vegetation indices of forested regions. *Remote Sens. Environ.* **1997**, *61*, 139–149. [CrossRef]
73. Zhang, L.; Han, W.; Niu, Y.; Chávez, J.L.; Shao, G.; Zhang, H. Evaluating the sensitivity of water stressed maize chlorophyll and structure based on UAV derived vegetation indices. *Comput. Electron. Agric.* **2021**, *185*, 106174. [CrossRef]
74. Mejias-Barrera, P. Effect of Reduced Irrigation on Grapevine Physiology, Grape Characteristics and Wine Composition in Three Pinot Noir Vineyards with Contrasting Soils. Ph.D. Thesis, Lincoln University, Lincoln, New Zealand, 2016.
75. Baluja, J.; Diago, M.P.; Balda, P.; Zorer, R.; Meggio, F.; Morales, F.; Tardaguila, J. Assessment of vineyard water status variability by thermal and multispectral imagery using an unmanned aerial vehicle (UAV). *Irrig. Sci.* **2012**, *30*, 511–522. [CrossRef]
76. Matese, A.; Baraldi, R.; Berton, A.; Cesaraccio, C.; Di Gennaro, S.F.; Duce, P.; Facini, O.; Mameli, M.G.; Piga, A.; Zaldei, A. Combination of proximal and remote sensing methods for mapping water stress conditions of grapevine. In *International Symposium on Sensing Plant Water Status—Methods and Applications in Horticultural Science*; ISHS: Leuven, Belgium, 2016.
77. Hunt, E.R., Jr.; Hively, W.D.; Fujikawa, S.J.; Linden, D.S.; Daughtry, C.S.; McCarty, G.W. Acquisition of NIR-green-blue digital photographs from unmanned aircraft for crop monitoring. *Remote Sens.* **2010**, *2*, 290–305. [CrossRef]
78. Boiarskii, B.; Hasegawa, H. Comparison of NDVI and NDRE indices to detect differences in vegetation and chlorophyll content. *J. Mech. Contin. Math. Sci.* **2019**, *4*, 20–29. [CrossRef]
79. Espinoza, C.Z.; Khot, L.R.; Sankaran, S.; Jacoby, P.W. High Resolution Multispectral and Thermal Remote Sensing-Based Water Stress Assessment in Subsurface Irrigated Grapevines. *Remote Sens.* **2017**, *9*, 961. [CrossRef]
80. Schultz, H.; Matthews, M. Vegetative Growth Distribution During Water Deficits in *Vitis vinifera* L. *Funct. Plant Biol.* **1988**, *15*, 641–656. [CrossRef]
81. Caruso, G.; Tozzini, L.; Rallo, G.; Primicerio, J.; Moriondo, M.; Palai, G.; Gucci, R. Estimating biophysical and geometrical parameters of grapevine canopies ('Sangiovese') by an unmanned aerial vehicle (UAV) and VIS-NIR cameras. *Vitis* **2017**, *56*, 63–70.
82. Junges, A.H.; Fontana, D.C.; Anzanello, R.; Bremm, C. Normalized difference vegetation index obtained by ground-based remote sensing to characterize vine cycle in Rio Grande do Sul, Brazil. *Ciência Agrotecnologia* **2017**, *41*, 543–553. [CrossRef]
83. Elfving, D.C.; Kaufmann, M.R.; Hall, A.E. Interpreting Leaf Water Potential Measurements with a Model of the Soil-Plant-Atmosphere Continuum. *Physiol. Plant.* **1972**, *27*, 161–168. [CrossRef]
84. Rodríguez, J.C.; Grageda, J.; Watts, C.J.; Garatuza-Payan, J.; Castellanos-Villegas, A.; Rodríguez-Casas, J.; Saiz-Hernandez, J.; Olavarrieta, V. Water use by perennial crops in the lower Sonora watershed. *J. Arid. Environ.* **2010**, *74*, 603–610. [CrossRef]

85. Gutiérrez-Gamboa, G.; Pérez-Donoso, A.G.; Pou-Mir, A.; Acevedo-Opazo, C.; Valdés-Gómez, H. Hydric behaviour and gas exchange in different grapevine varieties (*Vitis vinifera* L.) from the Maule Valley (Chile). *S. Afr. J. Enol. Vitic.* **2019**, *40*. [CrossRef]
86. Bellvert, J.; Marsal, J.; Mata, M.; Girona, J. Identifying irrigation zones across a 7.5-ha 'Pinot noir'vineyard based on the variability of vine water status and multispectral images. *Irrig. Sci.* **2012**, *30*, 499–509. [CrossRef]
87. Yu, R.; Brillante, L.; Martínez-Lüscher, J.; Kurtural, S.K. Spatial Variability of Soil and Plant Water Status and Their Cascading Effects on Grapevine Physiology Are Linked to Berry and Wine Chemistry. *Front. Plant Sci.* **2020**, *11*, 790. [CrossRef] [PubMed]
88. Lal, R.; Shukla, M.R. *Principles of Soil Physics, Part II*; Marcel Dekker: New York, NY, USA, 2004; pp. 182–223. [CrossRef]
89. Zhu, Q.; Lin, H.; Doolittle, J. Repeated Electromagnetic Induction Surveys for Determining Subsurface Hydrologic Dynamics in an Agricultural Landscape. *Soil Sci. Soc. Am. J.* **2010**, *74*, 1750–1762. [CrossRef]
90. Callegary, J.B.; Ferré, T.P.; Groom, R. Three-dimensional sensitivity distribution and sample volume of low-induction-number electromagnetic-induction instruments. *Soil Sci. Soc. Am. J.* **2012**, *76*, 85–91. [CrossRef]
91. Keller, M. *The Science of Grapevines*; Academic Press: Cambridge, MA, USA, 2020.
92. Jarvis, P.G.; McNaughton, K.G. Stomatal Control of Transpiration: Scaling Up from Leaf to Region. *Adv. Ecol. Res.* **1986**, *15*, 1–49. [CrossRef]
93. Kobriger, J.; Kliewer, W.; Lagier, S. Effects of wind on water relations of several grapevine cultivars. *Am. J. Enol. Vitic.* **1984**, *35*, 164–169.
94. Campbell-Clause, J. Stomatal response of grapevines to wind. *Aust. J. Exp. Agric.* **1998**, *38*, 77–82. [CrossRef]
95. Schymanski, S.J.; Or, D. Wind increases leaf water use efficiency. *Plant Cell Environ.* **2016**, *39*, 1448–1459. [CrossRef] [PubMed]
96. Spiess, A.-N.; Neumeyer, N. An evaluation of R2 as an inadequate measure for nonlinear models in pharmacological and biochemical research: A Monte Carlo approach. *BMC Pharmacol.* **2010**, *10*, 6. [CrossRef] [PubMed]
97. Tange, R.I.; Rasmussen, M.A.; Taira, E.; Bro, R. Benchmarking support vector regression against partial least squares regression and artificial neural network: Effect of sample size on model performance. *J. Near Infrared Spectrosc.* **2017**, *25*, 381–390. [CrossRef]
98. Adams, H.D.; Williams, A.P.; Xu, C.; Rauscher, S.A.; Jiang, X.; McDowell, N.G. Empirical and process-based approaches to climate-induced forest mortality models. *Front. Plant Sci.* **2013**, *4*, 438. [CrossRef]